Electric field induced tunable half-metallicity in an *A*-type antiferromagnetic bilayer $LaBr_2$

Qingqing Chen [1,2] Xiaohong Zheng [3,*] Peng Jiang,[4,†] Yan-Hong Zhou,[5] Lei Zhang,[6,7,‡] and Zhi Zeng[1,2]

[1] *Key Laboratory of Materials Physics, Institute of Solid State Physics, HFIPS, Chinese Academy of Sciences, Hefei 230031, China*
[2] *Science Island Branch of Graduate School, University of Science and Technology of China, Hefei 230026, China*
[3] *College of Information Science and Technology, Nanjing Forestry University, Nanjing 210037, China*
[4] *School of Physics and Electronic Engineering, Jiangsu Normal University, Xuzhou 221116, China*
[5] *College of Science, East China Jiao Tong University, Nanchang 330013, China*
[6] *State Key Laboratory of Quantum Optics and Quantum Optics Devices, Institute of Laser Spectroscopy, Shanxi University, Taiyuan 030006, China*
[7] *Collaborative Innovation Center of Extreme Optics, Shanxi University, Taiyuan 030006, China*

(Received 28 July 2022; revised 8 November 2022; accepted 5 December 2022; published 21 December 2022)

How to achieve half-metallicity is always a central topic in spintronics and the polarity-tunable half-metallicity is particularly interesting for spin manipulation. In this work, motivated by the intrinsic ferromagnetism in the monolayer electride $LaBr_2$, based on density functional theory calculations, we investigate the electronic and magnetic properties of bilayer $LaBr_2$, with an aim to search for polarity-tunable half-metallicity. We first find that the antiferromagnetic interlayer coupling state is the ground state and the band structure is spin degenerate, with an indirect band gap of 0.454 eV. By applying a vertical electric field, spin splitting occurs and when the electric field is strong enough ($\geqslant$0.33 V/Å), half-metallicity can be achieved. More interestingly, the spin polarity of the half-metallicity can be tuned by reversing the electric field direction. It originates from the spatial separation of the two spin channels in both the valence band and conduction band and their localization at different layers. Based on the polarity-tunable half-metallicity under vertical electric field, a magnetic tunnel junction based on bilayer $LaBr_2$ is designed and the ON/OFF switching can be achived by applying parallel or anti-parallel vertical electric fields in the two leads, which leads to giant tunnel magnetoresistance up to 1×10^6. The findings suggest new potential of $LaBr_2$, and more generally, *A*-type antiferromagnets of application in spintronic devices.

DOI: 10.1103/PhysRevB.106.245423

I. INTRODUCTION

As microelectronic devices approach their size limits, Joule heat will become a serious problem in the semiconductor industry since the resulting high temperature in the electronic units will severely degrade their performance. As a result, devices working on new mechanisms and generating much less Joule heat are important solutions to the above problem. Spintronics or spin-based electronics, which focuses on using the spin degree of freedom of electron instead of charge as the information carrier, offers great opportunities for next generation information technology with the advantages of low energy consumption, fast device operation, and high storage density [1,2]. For spintronic devices at nanoscale, atomically thin two-dimensional (2D) ferromagnetic materials with the combination of large spin polarization and high Curie temperature (T_c) are of particular importance and interest [3–5]. As a matter of fact, 2D materials provide excellent candidate building blocks for future electronic devices due to their atomically thin thickness and the subsequent ability to meet the continuous miniaturization demand [6–8]. Nevertheless, due to thermal fluctuations and weak magnetic anisotropy energy, it has been long considered that no spontaneous long-range magnetic order would occur in a two-dimensional system [9]. Starting from 2017, experimental researchers successively observed many two-dimensional materials with intrinsic magnetism, such as $Gr_2Ge_2Fe_6$, CrI_3, VSe_2, $CrGeTe_3$, Fe_3GeTe_2, $NiPS_3$, CoH_2 and $CrBr_3$ [7,10–15]. The discovery of these 2D magnetic materials greatly enhances the development of spintronics in the field of low dimensional systems.

It is well known that spin polarization is at the heart of spintronics and traditionally spin-polarized current can be realized by current injection from ferromagnets [16–19] magnetic semiconductors [20–22] or materials with a giant Zeeman spin splitting [23–25]. Needless to say, spin polarization itself is not rare and it can be observed in any magnetic system. The aim of numerous studies thus far is to achieve high spin polarization since we need the difference between the two spin channels to be as large as possible practically. In this regard, half-metallic transport is particularly interesting due to its 100% spin polarization. However, the realization of half-metallicity is much more challenging and the intrinsic half-metallicity as characterized by a single spin channel around the Fermi level in the band structure has only been observed in a limited number of materials [26–28]. Actually, besides intrinsic half-metallicity, a lot of schemes have been proposed to extrinsically achieve half-metallic transport, such

*xhzheng@njfu.edu.cn
†pjiang@jsnu.edu.cn
‡zhanglei@sxu.edu.cn

 ©2022 American Physical Society

as electric field [29], edge decoration [30,31], impurity doping [32–34] and construction of van der Waals heterostructures [35] combined with photogalvanic effect [36] and ferroelectric control [37], etc.

Additionally, whether it is possible further to control the carrier's spin orientation or the spin polarity of the half-metallicity is also a key issue for spintronics. For conventional half-metals, spin polarization is fixed in a specific direction, that is, either spin up or spin down. It is natural that switching between the two spin directions can be achieved by spontaneous magnetization reversals under an external magnetic field, but unfortunately magnetic control with nanoscale precision is generally very difficult. The half-metallicity obtained with external control means such as edge decoration and impurity doping is also hard to reverse. Comparatively, electric control of carrier spin polarization at nanoscale is much easier and has attracted great attention [38–41]. In 2006, Louie *et al.* realized half-metallicity in zigzag-edged graphene nanoribbons with a transverse electric field based on the facts that that the two edges of graphene nanoribbons are antiferromagnetically coupled and the edge states of different spin channels are spatially separated at different edges, which allows it to conveniently tune the energy of different edge states and the related spin subbands by an electric field [29]. In 2018, Gong *et al.* realized half-metallicity in bilayer VSe_2 *A*-type antiferromagnetic structure by applying vertically an electric field to it [42]. The feature in common for both the schemes of Louie and Gong is that the two spin channels in either the valence band or the conduction band are spatially distributed at different positions, so that the energy of them can be shifted towards opposite directions by an electric field and their relative shift direction can be easily controlled by reversing the electric field.

In this work, based on first-principles calculations, we investigate the electrical control of spin polarization in a newly discovered bilayer $LaBr_2$, with an aim to achieve half-metallicity and the control of its spin polarity. Previous studies have shown that single layer $LaBr_2$ is a stable ferromagnetic material [43,44]. Similar properties can be observed in other two-dimensional systems, such as LaBrI, CeI_2, $GdBr_2$ [45–47]. We find that, for bilayer $LaBr_2$, the intralayer coupling is ferromagnetic, while the interlayer coupling is antiferromagnetic, i.e., bilayer $LaBr_2$ is an *A*-type antiferromagnetic semiconductor. Further we demonstrate that the bilayer $LaBr_2$ can be driven to be half metal by a vertical electric field and the spin polarity can be exchanged by reversing the electric field. Based on these findings, we propose to construct a magnetic tunnel junction with bilayer $LaBr_2$, in which giant tunnel magnetoresistance (TMR) can be achieved by applying parallel and antiparallel electric fields in the two leads, respectively.

II. CALCULATIONAL DETAILS

The calculations for structure optimization, electronic structure, and magnetism are carried out using density functional theory (DFT) as implemented in the Vienna *ab initio* Simulation Package (VASP) [48–50]. The exchange correlation interactions are described by the generalized gradient approximation of the Perdew-Burke-Ernzerhof form, and the projector-augmented plane wave potentials [51,52]. A Hubbard U value of 5.5 eV was used for $4f$ orbitals of La atoms to consider the correlation effect from it [53]. The energy cutoff of plane wave expansion is chosen to be 500 eV. A $12\times12\times1$ Monkhorst-Pack k-point mesh was used to sample the Brillouin zone and the Gaussian smearing width of 0.05 eV was adopted. A vacuum region of 30 Å in the vertical direction was used in the structural relaxation calculations of the central regions to avoid interaction between adjacent slabs. Moreover, van der Waals force was considered through the DFT-D2 method in all the structural optimizations [54,55]. The convergence criteria for force and total energy are chosen as 0.001 eV/Å and 10^{-6} eV, respectively.

The calculations of quantum transport are performed using Nanodcal package based on real-space DFT combined with non-equilibrium Green's function formalism [56]. The spin-resolved conductance is calculated by

$$G_\sigma = \frac{e^2}{\hbar} T_\sigma(E_F, V=0), \tag{1}$$

with

$$T_\sigma(E, V) = \sum_{k_{//}} T_\sigma(E, k_{//}, V), \tag{2}$$

where e is the electron charge, h is the Planck constant, and $T_\sigma(E_F, k_{//}, V)$ is the spin-resolved transmission coefficient with spin $\sigma(\sigma = \uparrow, \downarrow)$ at energy E and transverse Bloch wave vector $k_{//} = (k_x, k_y)$ under bias V. For similicity, the index $k_{//}$ will be omitted below. For each $k_{//}$ point, the transmission function is calculated by

$$T_\sigma(E, V) = Tr[\Gamma_L(E, V)G^R(E, V)\Gamma_R(E, V)G^A(E, V)]_\sigma, \tag{3}$$

where $G^{R(A)}$ is the retarded (advanced) Green's function of the central region and $\Gamma_{L(R)}$ is the linewidth function of left (right) electrode which describes the coupling between the electrode and the central scattering region. The current is calculated by

$$I_\sigma(V) = \frac{e}{\hbar} \int dET(E, V)[f_L(E) - f_R(E)], \tag{4}$$

where f_L and f_R are the Fermi distribution functions at energy E in the left and right electrodes, respectively.

III. RESULTS AND DISCUSSION

Similar to the structure of monolayer H-MoS_2, monolayer H-$LaBr_2$ possesses a honeycomb lattice, where one La atom layer is sandwiched between two hexagonal Br layers in a trigonal prismatic coordination, as shown in Fig. 1(a). The single-layer $LaBr_2$ is a thermodynamically stable ferromagnetic electride. Considering the valences of La^{3+} and Br^-, an extra electron is trapped in the crystal lattice gap in $LaBr_2$, which is the origin of the magnetic moment of this material [43,44]. Similar properties can be observed in other two-dimensional systems, such as LaBrI, CeI_2, and $GdBr_2$ [45–47]. Based on the unique properties of single layer $LaBr_2$, we put forward the two-layer structure as shown in Fig. 1(b). The optimized lattice constants are $a = b = 4.091$ Å, and the distance between the two layers is $d_{FM} = d_{AFM} = 3.136$ Å, which is close to the previous studies

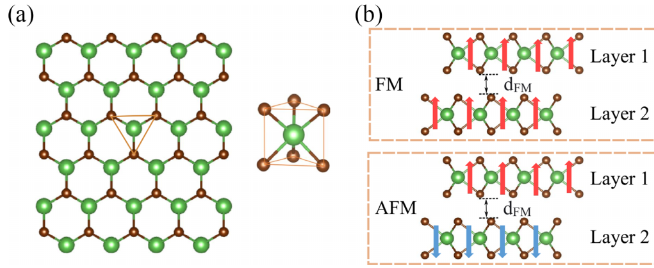

FIG. 1. (a) The structure of single layer $LaBr_2$, with the top view (left) and the side view (right). (b) The bilayer $LaBr_2$ and its FM and AFM configurations. The arrows indicate the directions of magnetic moments in each layer.

[57,58]. Next, we investigate the magnetic properties and the most stable magnetic configuration is determined by comparing the total energy of two different collinear magnetic structures, namely ferromagnetic(FM) and antiferromagnetic (AFM). Our results show that the total energy of AFM state is lower by 3.25 meV/f.u. than the FM state.

After having understood the two magnetic configurations, we investigate the electronic properties of the AFM state. The calculated electronic band structure [Fig. 2(a)] indicates that the 2D bilayer $LaBr_2$ crystal is a semiconductor with an indirect band gap of 0.454 eV. From the calculated wave functions of two bands around the Fermi level at the Γ point as shown in Fig. 2(b), it can be concluded that the spin-up valence band state ($v_\uparrow$) is located at Layer 2 (bottom layer), while the spin- down valence band state ($v_\downarrow$) is located at Layer 1 (top layer). In contrast, the spin-up conduction band state ($c_\uparrow$) is located at Layer 1, while spin-down conduction band state ($c_\downarrow$) is located at Layer 2. The layer resolved band structures of Layer 1 [Fig. 2(c)] and Layer 2 [Fig. 2(d)]

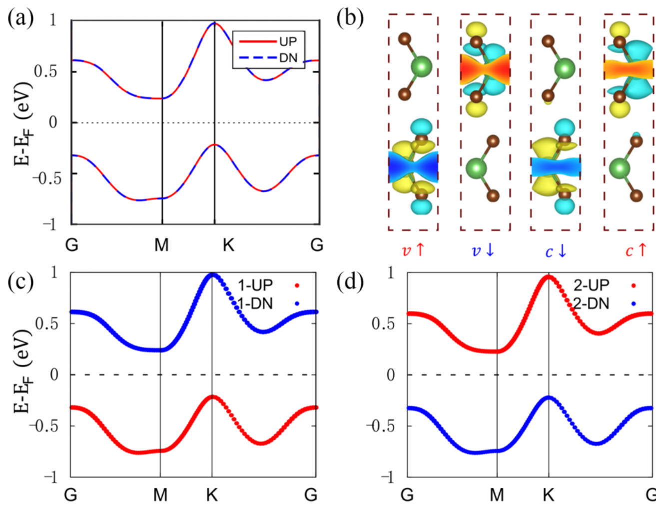

FIG. 2. (a)The band structure of the bilayer $LaBr_2$ with zero electric field. (b) The wave functions of different spin channels for the valence band and the conduction band at the Gamma point (with v and c denoting the valence band and conduction band, and ↑ and ↓ denoting spin up and spin down, respectively). (c) The layer resolved band structure of Layer 1. (d) The layer resolved band structure of Layer 2.

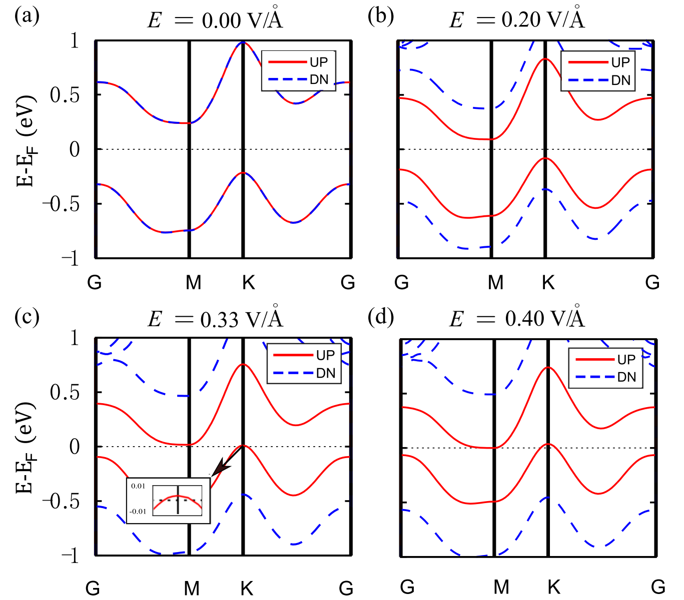

FIG. 3. The band structure of the bilayer $LaBr_2$ under different vertical electric field: (a) 0.0 V/Å; (b) 0.20 V/Å; (c) 0.33 V/Å; (d) 0.40 V/Å. All the first layer bands are pushed up, and the second layer bands are pushed down. Under critical field of 0.33 V/Å, the spin-up valence band in the first layer crosses the Fermi level, leading to half-metallicity. The inset in (c) shows the local part at the Fermi level around the Γ point.

further confirm the above distribution features. Such a spatial distribution of different spin channels in each band localized at different layers provides conditions for electric field regulation over their energies to induce difference between them. For example, when we apply apply an electric field $\vec{\varepsilon}$ directing from bottom to top, the additional electric potential energy ΔE arising from the external electric field will lead to the relative energy increase of Layer 1 and the relative energy decrease of Layer 2 according to $\Delta E = -eV(\vec{r})$, with $V(\vec{r})$ the interlayer potential drop. This will cause the shift of the spin-up channel in both layers to the Fermi level while the shift of the spin-down channel in both layers is away from the Fermi level. If the electric field is strong enough, the spin up channel can be shifted to the Fermi level, leading to spin-up half-metallicity. On the contrary, if the direction of the electric field is reversed, the spin-down channel can be shifted to the Fermi level, leading to spin- down half-metallicity.

Based on the above analysis, the bilayer $LaBr_2$ band structures are calculated at different electric field. Considering that crystal structure may change by electric field, the structure has been fully relaxed under each electric field. From Figs. 3(a)–3(d), when an electric field is applied, spin splitting occurs and it becomes larger with the increase of field strength. At $\varepsilon = 0.33$ V/Å, both the valence band maximum and the conduction band minimum of the spin-up channel touch the Fermi level simultaneously, leading to 100% spin polarization around the Fermi level.

In order to gain further insight into the relationship between half metallicity and electric field, we draw the band gap

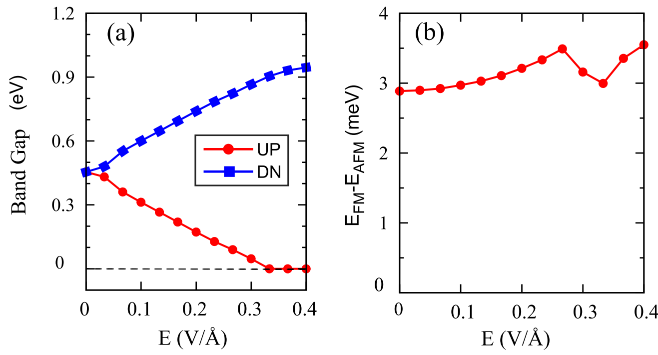

FIG. 4. (a) Electric field dependence of the band gap. (b)The total energy difference between the ferromagnetic and antiferromagnetic interlayer couplings as a function of electric field.

changes of both spin channels as a function of the electric field in Fig. 4(a). It is seen that the band gap of the spin-up band gradually decreases with the increase of the electric field. When it exceeds the critical electric field (0.33 V/Å), the spin-up band gap becomes zero, and the spin-up channel is converted to metal. On the other hand, the band gap of spin down increases gradually with the electric field. We have also compared the energy difference of the two magnetic configurations as a function of the electric field, as shown in Fig. 4(b). It is found that in the whole applied electric field range of $0 \sim 0.40$ V/Å[Fig. 4(b)], the total energy difference always keeps $E_{\mathrm{FM}} - E_{\mathrm{AFM}} > 0$, which indicates that the interlayer coupling of the ground state is always AFM. Before it gets close to the critical electric field of 0.33 V/Å, the applied electric field can cause electron polarization inside one layer, but cannot cause charge transfer between layers. When it gets close the critical value, although the whole system is electrically neutral, charge transfer begins to occur between layers. Since the valence band and the conduction band crossing the Fermi level have the same spin orientation but are from different layers, charge transfer between them increases the proportion of interlayer ferromagnetic coupling, which causes the decrease of the FM-AFM energy difference around the critical value [see Fig. 4(b)], but the system still stays on the AFM state even if the electric field is as large as 0.40 V/Å. Interestingly, if the direction of the electric field is reversed, the bands crossing the Fermi level will be from the spin down channel, meaning that the spin polarity of the half-metallicity is switchable.

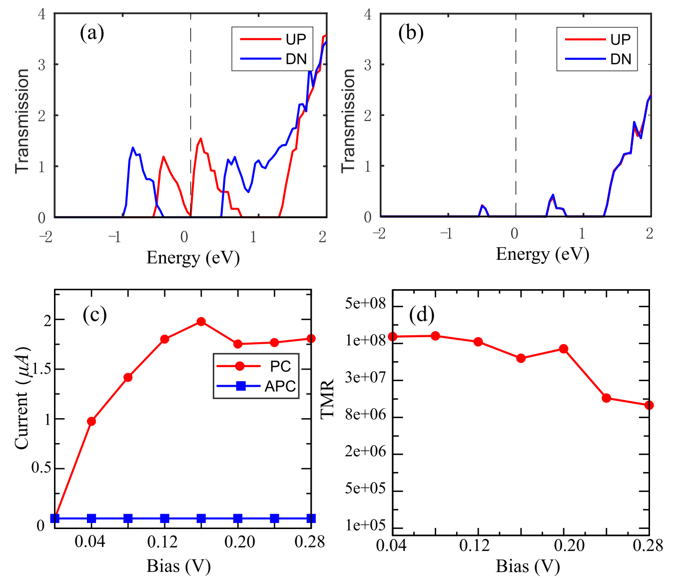

FIG. 6. The transmission functions for the case: (a) PC; (b) APC with $V_g = 10$ V. (c) I–V curve under PC and APC. (d) TMR of the system at small bias.

Taking advantage of these characteristics, a magnetic tunnel junction is designed as shown in Fig. 5, in which the infinite bilayer $\mathrm{LaBr_2}$ is divided into three regions: left lead, central region, and right lead. The central region includes nine unit cells along the transport direction. To tune the transport properties, electric field is applied vertically to both leads. We consider two configurations of the electric field in the two leads. In the parallel configuration (PC), the electric fields in both leads point downward, while in the antiparallel configuration (APC), the electric field in the left lead points downward and that in the right lead points upward. In the PC, since the half-metallic carriers of the left and right leads are both spin-up electrons, spin-up current can flow through the device. We call this an “ON″ state. On the contrary, by reversing the direction of the electric field of the right lead, around the Fermi level, the left lead has spin-up electrons while the right lead has spin down electrons. Due to the spin mismatch, both spin channels will be blocked. This is called an “OFF” state. Consequently, a giant tunnel magnetoresistance will be achieved. For the device designed above, its transmission functions are calculated for the two PC and APC cases, with $V_g = 10$ V, as shown in Figs. 6(a) and 6(b). It is seen that there

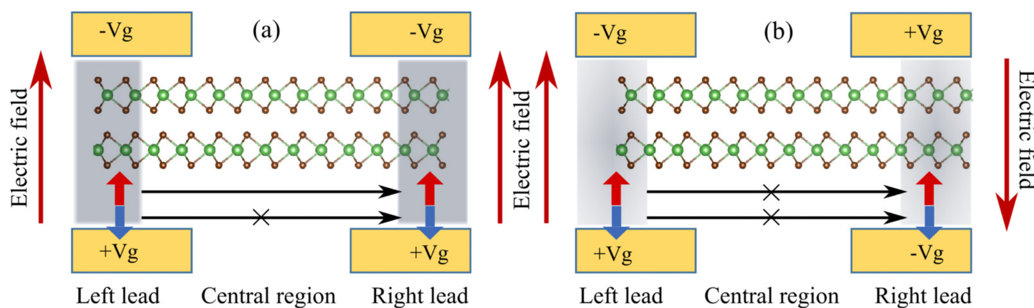

FIG. 5. Magnetic tunnel junction constructed with bilayer $\mathrm{LaBr_2}$, with both leads under an electric field for the case: (a) PC; (b) APC. The yellow areas indicate the gate regions. The horizontal arrows indicate the open or closed spin channels.

are two spin-up transmission peaks around the Fermi level for the PC case, and the spin-down transmission is zero, thus the spin polarization $\eta = |\frac{T^{\uparrow}-T^{\downarrow}}{T^{\uparrow}+T^{\downarrow}}|$ approaches 100%. For the APC case, both spin channels are nearly completely blocked, as predicted. Figures 6(c) and 6(d) show the I-V curve with bias ranging from 0.0 to 0.28 V and the corresponding TMR of the system as defined by TMR $= \frac{I_{\mathrm{PC}}-I_{\mathrm{APC}}}{I_{\mathrm{APC}}}$ under small bias. Due to the symmetry of the system, only the results of the forward voltage are presented. With the increase of bias, the current under PC case increases rapidly first until 0.16 V and then it approaches a stable value, while the current of APC case always maintains a negligibly small value, which results in the TMR higher than $10^6 \sim 10^8$. These results are consistent with our expectations. It is much larger than that [of the order $(1 \sim 100)$] generally reported in other 2D materials based magnetic tunnel junctions (MTJs) [59], but comparable to that ($10^6 \sim 10^7$) in MXene-Based $Mn_2CF_2/Ti_2CO_2/Mn_2CF_2$ MTJs [60] and zigzag graphene nanoribbon based MTJs [61]. Certainly, the experimental TMR ratios are usually lower than calculated values due to the nonzero temperature and the possible defect scattering in experiments [62,63].

IV. SUMMARY

We have investigated the electronic structure and magnetic properties of bilayer $LaBr_2$ and found that its ground state is an *A*-type antiferromagnet, with an indirect band gap of 0.454 eV and FM-AFM energy difference of 3.25 meV/f.u.. Wave functions and layer resolved band structures reveal that the spin-up valence band and spin-down conduction band are contributed by the bottom layer, while the spin-down valence band and spin-up conduction band are contributed by the top layer. Such a spatial separation feature makes it very easy to tune the energy of different spin channels in different layers by a vertical electric field, and especially half-metallicity can be achieved and the spin polarity of the half-metallicity can be exchanged by reversing the electric field. First- principles calculations indicate that the critical field to achieve half-metallicity is 0.33 V/Å. Based on the electric field effects on the electronic structure of the bilayer $LaBr_2$, a magnetic tunnel junction with giant magnetoresistence can be constructed and our calculations indicate that not only half-metallic transport can be achieved, but also a TMR ratio as high as 10^6 at small bias can be obtained by controlling the vertical electric field applied to the leads. These findings suggest the additional possibility of $LaBr_2$ in the design of spintronic devices.

ACKNOWLEDGMENTS

We gratefully acknowledge financial support by the National Natural Science Foundation of China (Grants No. 11974355, No. 12204202, No. 12074230, and No. 12264014); Shanxi Province 100-Plan Talent Program and the Fund for Shanxi "1331 Project"; the Natural Science Foundation of Jiangsu Province (Grant No. BK20220679); the Natural Science Fund for Colleges and Universities in Jiangsu Province (Grant No. 22KJB140010); and the Natural Science Foundation of Jiangxi Province (Grant No. 20202ACBL212005). Calculations were performed in the Center for Computational Science of CASHIPS, the ScGrid of Supercomputing Center and Computer Network Information Center of Chinese Academy of Sciences, and Hefei advanced computing center.

[1] A. Fert, Nobel Lecture: Origin, development, and future of spintronics, Rev. Mod. Phys. **80**, 1517 (2008).
[2] C. Felser, G. H. Fecher, and B. Balke, Spintronics: A challenge for materials science and solid-state chemistry, Angew. Chem. Int. Ed. **46**, 668 (2007).
[3] C. Tan, X. Cao, X. Wu, Q. He, J. Yang, X. Zhang, J. Chen, W. Zhao, S. Han, G. Nam *et al.*, Recent advances in ultrathin two-dimensional nanomaterials, Chem. Rev. **117**, 6225 (2017).
[4] N. Miao, B. Xu, N. C. Bristowe, J. Zhou, and Z. Sun, Tunable magnetism and extraordinary sunlight absorbance in indium triphosphide monolayer, J. Am. Chem. Soc. **139**, 11125 (2017).
[5] W. Cheng, J. He, T. Yao, Z. Sun, Y. Jiang, Q. Liu, S. Jiang, F. Hu, Z. Xie, B. He *et al.*, Half-unit-cell α-Fe_2O_3 semiconductor nanosheets with intrinsic and robust ferromagnetism, J. Am. Chem. Soc. **136**, 10393 (2014).
[6] K. S. Novoselov, A. K. Geim, S. V. Morozov, D. Jiang, Y. Zhang, S. V. Dubonos, I. V. Grigorieva, and A. A. Firsov, Electric field effect in atomically thin carbon films, Science **306**, 666 (2004).
[7] C. Gong, L. Li, Z. Li, H. Ji, A. Stern, Y. Xia, T. Cao, W. Bao, C. Wang, and Y. Wang, Discovery of intrinsic ferromagnetism in two-dimensional van der Waals crystals, Nature (London) **546**, 265 (2017).
[8] W. Han, Perspectives for spintronics in 2D materials, APL Mater. **4**, 032401 (2016).
[9] N. D. Mermin and H. Wagner, Absence of Ferromagnetism or Antiferromagnetism in One- or Two-Dimensional Isotropic Heisenberg Models, Phys. Rev. Lett. **17**, 1133 (1966).
[10] B. Huang, G. Clark, E. Navarro-Moratalla, D. R. Klein, R. Cheng, K. L. Seyler, D. Zhong, E. Schmidgall, M. A. Mcguire, and D. H. A. Cobden, Layer-dependent ferromagnetism in a van der Waals crystal down to the monolayer limit, Nature (London) **546**, 270 (2017).
[11] M. Bonilla, S. Kolekar, Y. Ma, H. C. Diaz, V. Kalappattil, R. Das, T. Eggers, H. R. Gutierrez, M. Phan, and M. Batzill, Strong room-temperature ferromagnetism in VSe_2 monolayers on van der Waals substrates, Nat. Nanotechnol. **13**, 289 (2018).
[12] Y. Deng, Y. Yu, Y. Song, J. Zhang, N. Z. Wang, Z. Sun, Y. Yi, Y. Z. Wu, S. Wu, J. Zhu *et al.*, Gate-tunable room-temperature ferromagnetism in two-dimensional Fe_3GeTe_2, Nature (London) **563**, 94 (2018).
[13] N. Miao, B. Xu, L. Zhu, Z. Jian, and Z. Sun, 2D Intrinsic Ferromagnets from van der Waals Antiferromagnets, J. Am. Chem. Soc. **140**, 2417 (2018).
[14] Q. Wu, Y. Zhang, Q. Zhou, J. Wang, and X. C. Zeng, Transition-metal dihydride monolayers: A new family of two-dimensional ferromagnetic materials with intrinsic room-temperature half-metallicity, J. Phys. Chem. Lett. **9**, 4260 (2018).
[15] C. Huang, Y. Du, H. Wu, H. Xiang, K. Deng, and E. Kan, Prediction of Intrinsic Ferromagnetic Ferroelectricity in

a Transition-Metal Halide Monolayer, Phys. Rev. Lett. **120**, 147601 (2018).

[16] P. R. Hammar, B. R. Bennett, M. J. Yang, and M. Johnson, Observation of Spin Injection at a Ferromagnet-Semiconductor Interface, Phys. Rev. Lett. **83**, 203 (1999).

[17] M. Johnson and R. H. Silsbee, Interfacial Charge-Spin Coupling: Injection and Detection of Spin Magnetization in Metals, Phys. Rev. Lett. **55**, 1790 (1985).

[18] A. N. Chantis, K. D. Belashchenko, D. L. Smith, E. Y. Tsymbal, M. van Schilfgaarde, and R. C. Albers, Reversal of Spin Polarization in Fe/GaAs (001) Driven by Resonant Surface States: First-Principles Calculations, Phys. Rev. Lett. **99**, 196603 (2007).

[19] C. A. Merchant and N. Marković, Electrically Tunable Spin Polarization in a Carbon Nanotube Spin Diode, Phys. Rev. Lett. **100**, 156601 (2008).

[20] Y. Ohno, D. Young, B. A. Beschoten, F. Matsukura, H. Ohno, and D. Awschalom, Electrical spin injection in a ferromagnetic semiconductor heterostructure, Nature (London) **402**, 790 (1999).

[21] T. Dietl and H. Ohno, Dilute ferromagnetic semiconductors: Physics and spintronic structures, Rev. Mod. Phys. **86**, 187 (2014).

[22] K. Sato, L. Bergqvist, J. Kudrnovský, P. H. Dederichs, O. Eriksson, I. Turek, B. Sanyal, G. Bouzerar, H. Katayama-Yoshida, V. A. Dinh, T. Fukushima, H. Kizaki, and R. Zeller, First-principles theory of dilute magnetic semiconductors, Rev. Mod. Phys. **82**, 1633 (2010).

[23] R. Jansen, B. C. Min, and S. P. Dash, Oscillatory spin-polarized tunnelling from silicon quantum wells controlled by electric field, Nat. Mater. **9**, 133 (2010).

[24] I. Žutić, J. Fabian, and S. Das Sarma, Spintronics: Fundamentals and applications, Rev. Mod. Phys. **76**, 323 (2004).

[25] R. Fiederling, M. Keim, G. A. Reuscher, W. Ossau, G. Schmidt, A. Waag, and L. Molenkamp, Injection and detection of a spin-polarized current in a light-emitting diode, Nature (London) **402**, 787 (1999).

[26] R. A. de Groot, F. M. Mueller, P. G. van Engen, and K. H. J. Buschow, New Class of Materials: Half-Metallic Ferromagnets, Phys. Rev. Lett. **50**, 2024 (1983).

[27] X. Li, X. Wu, and J. Yang, Room-temperature half-metallicity in La (Mn, Zn) AsO alloy via element substitutions, J. Am. Chem. Soc. **136**, 5664 (2014).

[28] X. Li, H. Lv, J. Dai, L. Ma, X. C. Zeng, X. Wu, and J. Yang, Half-metallicity in one-dimensional metal trihydride molecular nanowires, J. Am. Chem. Soc. **139**, 6290 (2017).

[29] Y. W. Son, M. L. Cohen, and S. G. Louie, Half-metallic graphene nanoribbons, Nature (London) **444**, 347 (2006).

[30] E.-J. Kan, Z. Li, J. Yang, and J. G. Hou, Half-metallicity in edge-modified zigzag graphene nanoribbons, J. Am. Chem. Soc. **130**, 4224 (2008).

[31] M. Wu, X. Wu, and X. C. Zeng, Exploration of half metallicity in edge-modified graphene nanoribbons, J. Phys. Chem. C **114**, 3937 (2010).

[32] S. Dutta, A. K. Manna, and S. K. Pati, Intrinsic Half-Metallicity in Modified Graphene Nanoribbons, Phys. Rev. Lett. **102**, 096601 (2009).

[33] X. H. Zheng, X. L. Wang, T. A. Abtew, and Z. Zeng, Building half-metallicity in graphene nanoribbons by direct control over edge states occupation, J. Phys. Chem. C **114**, 4190 (2010).

[34] P. Jiang, L. Kang, X. Zheng, Z. Zeng, and S. Sanvito, Computational prediction of a two-dimensional semiconductor SnO_2 with negative Poisson's ratio and tunable magnetism by doping, Phys. Rev. B **102**, 195408 (2020).

[35] J. Yu and W. Guo, A new paradigm to half-metallicity in graphene nanoribbons, J. Phys. Chem. Lett. **4**, 951 (2013).

[36] X. Tao, L. Zhang, X. Zheng, H. Hao, X. Wang, L. Song, Z. Zeng, and H. Guo, h-BN/graphene van der Waals vertical heterostructure: a fully spin-polarized photocurrent generator, Nanoscale **10**, 174 (2018).

[37] P. Jiang, L. Kang, H. Hao, X. Zheng, Z. Zeng, and S. Sanvito, Ferroelectric control of electron half-metallicity in *A*-type antiferromagnets and its application to nonvolatile memory devices, Phys. Rev. B **102**, 245417 (2020).

[38] Y. Kato, R. Myers, D. Driscoll, A. Gossard, J. Levy, and D. Awschalom, Gigahertz electron spin manipulation using voltage-controlled g-tensor modulation, Science **299**, 1201 (2003).

[39] X. Li, X. Wu, Z. Li, J. Yang, and J. Hou, Bipolar magnetic semiconductors: a new class of spintronics materials, Nanoscale **4**, 5680 (2012).

[40] X. Li, X. Wu, and J. Yang, Half-metallicity in $MnPSe_3$ exfoliated nanosheet with carrier doping, J. Am. Chem. Soc. **136**, 11065 (2014).

[41] L. Zhang, J. Chen, X. Zheng, B. Wang, L. Zhang, L. Xiao, and S. Jia, Gate-tunable large spin polarization in a few-layer black phosphorus-based spintronic device, Nanoscale **11**, 11872 (2019).

[42] S. J. Gong, C. Gong, Y. Y. Sun, W. Y. Tong, C. G. Duan, J. H. Chu, and X. Zhang, Electrically induced 2D half-metallic antiferromagnets and spin field effect transistors, Proc. Natl. Acad. Sci. USA **115**, 8511 (2018).

[43] J. Zhou, Y. P. Feng, and L. Shen, Atomic-orbital-free intrinsic ferromagnetism in electrenes, Phys. Rev. B **102**, 180407(R) (2020).

[44] P. Zhao, Y. Ma, C. Lei, H. Wang, B. Huang, and Y. Dai, Single-layer $LaBr_2$: Two-dimensional valleytronic semiconductor with spontaneous spin and valley polarizations, Appl. Phys. Lett. **115**, 261605 (2019).

[45] P. Jiang, L. Kang, Y.-L. Li, X. Zheng, Z. Zeng, and S. Sanvito, Prediction of the two-dimensional Janus ferrovalley material LaBrI, Phys. Rev. B **104**, 035430 (2021).

[46] K. Sheng, Q. Chen, H. K. Yuan, and Z. Y. Wang, Monolayer CeI_2: An intrinsic room-temperature ferrovalley semiconductor, Phys. Rev. B **105**, 075304 (2022).

[47] W. Liu, J. Tong, L. Deng, B. Yang, G. Xie, G. Qin, F. Tian, and X. Zhang, Two-dimensional ferromagnetic semiconductors of rare-earth monolayer GdX_2 (X= Cl, Br, I) with large perpendicular magnetic anisotropy and high Curie temperature, Mater. Today Phys. **21**, 100514 (2021).

[48] G. Kresse and J. Furthmüller, Efficient iterative schemes for *ab initio* total-energy calculations using a plane-wave basis set, Phys. Rev. B **54**, 11169 (1996).

[49] G. Kresse and J. Hafner, *Ab initio* molecular dynamics for liquid metals, Phys. Rev. B **47**, 558 (1993).

[50] J. Taylor, H. Guo, and J. Wang, *Ab initio* modeling of quantum transport properties of molecular electronic devices, Phys. Rev. B **63**, 245407 (2001).

[51] J. P. Perdew, K. Burke, and M. Ernzerhof, Generalized Gradient Approximation Made Simple, Phys. Rev. Lett. **77**, 3865 (1996).

[52] P. E. Blöchl, Projector augmented-wave method, Phys. Rev. B **50**, 17953 (1994).

[53] M. Topsakal and R. Wentzcovitch, Accurate projected augmented wave (PAW) datasets for rare-earth elements (RE= La–Lu), Comput. Mater. Sci. **95**, 263 (2014).

[54] S. Grimme, Semiempirical GGA-type density functional constructed with a long-range dispersion correction, J. Comput. Chem. **27**, 1787 (2006).

[55] T. Bučko, J. Hafner, S. Lebegue, and J. G. Angyán, Improved description of the structure of molecular and layered crystals: ab initio DFT calculations with van der Waals corrections, J. Phys. Chem. A **114**, 11814 (2010).

[56] J. Zhang, B. Zhao, T. Zhou, Y. Xue, C. Ma, and Z. Yang, Strong magnetization and Chern insulators in compressed graphene/CrI_3 van der Waals heterostructures, Phys. Rev. B **97**, 085401 (2018).

[57] K. Krömer, M. Schulze, W. Urland, and G. Meyer, Three Bromides of Lanthanum: $LaBr_2$, La_2Br_5, and $LaBr_3$, Z. Anorg. Allg. Chem. **575**, 61 (1989).

[58] W. Sun, W. Wang, H. Li, X. Li, Z. Yu, Y. Bai, G. Zhang, and Z. Cheng, $LaBr_2$ bilayer multiferroic moiré superlattice with robust magnetoelectric coupling and magnetic bimerons, npj Comput. Mater. **8**, 159 (2022).

[59] L. Zhang, J. Zhou, H. Li, L. Shen, and Y. P. Feng, Recent progress and challenges in magnetic tunnel junctions with 2D materials for spintronic applications, Appl. Phys. Rev. **8**, 021308 (2021).

[60] E. Balcı, Ü Özden Akkuş, and S. Berber, High TMR in MXene-based $Mn_2CF_2/Ti_2CO_2/Mn_2CF_2$ magnetic tunneling junction, ACS Appl. Mater. Interfaces **11**, 3609 (2019).

[61] M. Zhou, H. Jin, and Y. Xing, In-Plane Dual-Gated Spin-Valve Device Based on the Zigzag Graphene Nanoribbon, Phys. Rev. Appl. **13**, 044006 (2020).

[62] S. Maekawa and T. Shinjo, *Spin Dependent Transport in Magnetic Nanostructures* (CRC Press, Boca Raton, FL, 2002).

[63] J. S. Moodera and G. Mathon, Spin polarized tunneling in ferromagnetic junctions, J. Magn. Magn. Mater. **200**, 248 (1999).